Effect of Defects Buried in Pentacene/Alkanethiol Self-Assembled Monolayer/Au Film on Its Electronic Properties Visualized by Scanning Tunneling Microscopy/Spectroscopy

Yasuhiko Terada, Noriaki Takeuchi, Shoji Yoshida, Atsushi Taninaka, Osamu Takeuchi, and Hidemi Shigekawa*

Institute of Applied Physics, CREST-JST, University of Tsukuba, Tsukuba, Ibaraki 307-8573, Japan

Received January 15, 2010; accepted February 18, 2010; published online August 20, 2010

We have used scanning tunneling microscopy/spectroscopy to visualize the spatial correlation between buried structural defects and observed electronic properties in organic device structures. As a typical structure of an organic field-effect transistor, we have prepared pentacene/alkanethiol self-assembled monolayer (SAM)/Au samples with or without defects associated with a gap state at the molecule/Au interface. The effect of the defects, which were hidden behind the pentacene overlayers, on the electronic properties of the SAM was clearly observed. The method used in this study has potential for evaluating the nanoscale correlation between electrical properties and hidden defects inside organic devices.

DOI: 10.1143/JJAP.49.08LB08

1. Introduction

Designing nanometer-sized devices requires a well-defined fabrication technique using ultrathin dielectric layers. Downsizing and speeding up of field-effect transistors, for example, have been achieved by reducing the thickness of gate insulator films to the nanoscale limit. Inorganic materials are commonly used for insulator films, but ultrathin-film processing gives rise to complex issues, such as a large leakage current via tunneling. On the other hand, organic materials have an intrinsically low conductivity and are the best candidates for dielectric films.[1)] Additionally, advances in chemical synthesis and fabrication have promoted the use of organic materials in electronic devices.

In particular, the use of a self-assembled monolayer (SAM) as a gate dielectric in organic transistors was pioneered by Vuillaume *et al.*[2)] and has attracted considerable attention. Previous studies revealed a leakage current of 10^{-8} A cm^{-2},[2)] which is sufficiently low for practical use. Despite their high potential,[3–5)] SAMs still have critical issues, such as low film quality and packing order. SAMs have intrinsic and extrinsic defects, through which semiconductor materials may penetrate into the substrate. Such penetration reduces the effective dielectric thickness and yields current paths with a low resistivity. These imperfections are undesirable not only because they may trigger a large leakage current but also because the charging arising from the leakage results in the disorder in interfacial potential, which greatly affects carrier transport.[6)] Therefore, significant effort has been made to fabricate defect-free SAMs with sufficiently high robustness and insulating quality.[7)]

In this context, there is increasing demand for the quantitative investigation of the correlation between structural disorders in SAM dielectrics, such as defects and pinholes, and the overall electronic transport properties of the devices. Structural defects have been evaluated by spatially averaged techniques, including the evaluation of tilt, order, and gauche defects by Fourier transform infrared spectrometer (FT-IR),[8)] electron transport analysis by electrochemistry,[8)] and the investigation of structural defects such as pinholes.[8,9)] Local probe techniques, such as scanning tunneling microscopy/spectroscopy (STM/STS), atomic force microscopy, lateral force microscopy, and Kelvin probe force microscopy, have also been used for the real-space analysis of, for example, the self-assembly mechanism,[10,11)] defect characterization,[11)] and interfacial charging.[12)] Although these techniques provide much valuable information, little is known of the direct microscopic correlation between structural defects in buried dielectric layers and electronic transport properties of device structures.

Here, we present the potential of STM/STS to visualize the effect of defects formed at a molecule/metal interface and hidden behind the molecular overlayers on the electronic properties of thin films. STS spectra are, in general, obtained by plotting the tunneling current I or tunneling conductance dI/dV versus voltage V between an STM tip and a sample. dI/dV corresponds to the local density of states (LDOS) of the sample, and its mapping gives the spatial distribution of the electronic structure. If nanoscale defects associated with gap states exist in a bulk or on a surface, they appear in the dI/dV image as localized spots. We artificially introduced defects into SAM dielectric layers and investigated the effect of the defect-induced electronic states hidden beyond the overlayers using STM/STS. As a typical system, we used a pentacene thin film deposited on alkanethiol SAM/Au samples.

2. Experimental Procedure

The nature of electronic states of the hybrid orbital between a single pentacene molecule and a gold atom was investigated by Repp *et al.*[13)] They observed a new peak of dI/dV close to the lowest unoccupied molecular orbital (LUMO) of the original pentacene and confirmed that the peak is due to the hybrid orbital between the pentacene LUMO and the Au 6s state by density-functional calculations. On the other hand, X-ray photoemission and STM studies[14)] showed that the oxidation of the alkanethiol terminus results in the desorption of alkanethiol, which is characterized by the presence of striped phases in SAMs at the initial stage of oxidation. In each striped phase, alkanethiol molecules are oriented with the chain axis parallel to the surface, and the SAM molecules in the striped phase no longer act as a physical barrier and allow direct contact between pentacene and Au. Therefore, when pentacene molecules are adsorbed on the SAM formed by the oxidized alkanethiol molecules, pentacene molecules in striped-phase regions are expected to

*E-mail address: hidemi@ims.tsukuba.ac.jp

form gap states. On this basis, we prepared samples with or without buried defects associated with gap states.

Au(111) substrates were prepared by thermal evaporation on mica in vacuum. SAMs at saturation coverage were prepared by immersing Au(111) for 12 h into either octanethiol (C8) or dodecanethiol (C12) solution in toluene (1 mM) and subsequent rinsing. Pentacene powder was placed in a ceramic crucible and thermally deposited on a SAM in vacuum (5.0×10^{-5} Torr) at a rate of 0.002 nm/s. The coverage was monitored using a quartz oscillator.

SAMs with defects were prepared by promoting the oxidation of alkanethiol molecules during the SAM formation on Au; prior to the SAM formation, the alkanethiol solutions were exposed to air for more than a month to increase the concentration of dissolved oxygen. Referential SAMs were prepared with alkanethiol solutions that were deoxygenated and dehydrated to suppress the oxidation.

STM and STS measurements were performed in ultrahigh vacuum. I–V curves were taken at grid points covering the scanning area. dI/dV images were obtained by plotting the numerically calculated value of dI/dV at each grid point.

3. Results and Discussion

3.1 Introduction of defects by oxidized alkanethiol molecules

First, we examined the introduction of defect into SAMs. To confirm their introduction, we observed a C8-SAM that had been subjected to oxidation promotion. Figure 1(a) shows an example STM image. Although most of the surface is covered by a saturation phase, a $c(4\times2)$ superlattice of a $(\sqrt{3}\times\sqrt{3})R$ 30° lattice [inset in Fig. 1(a)],[11] the following two types of defect were observed: One type comprises pitlike defects [marked as A in Fig. 1(a)], which are commonly observed for alkanethiol SAMs at saturation. Since they have the depth of the Au(111) single step height of 2.5 Å, they are assigned to islands of Au vacancies and not the defects in the SAM itself. The other type comprises stripe-phase (marked as B) in which alkanethiol molecules are oriented with the chain axis parallel to the surface. Figures 1(b) and 1(c) show wide-area images obtained for an oxidized sample and an oxidation-suppressed sample, where the stripe-phase defects, etch pits, and domain boundaries are drawn in red, blue, and green, respectively. As shown in Fig. 1(b), stripe phases (drawn in red) surround and connect etch pits or steps. On the other hand, as expected, the stripe phase was hardly observed in the reference SAM prepared with its oxidation suppressed [Fig. 1(c)], although etch pits and domain boundaries were still observed.

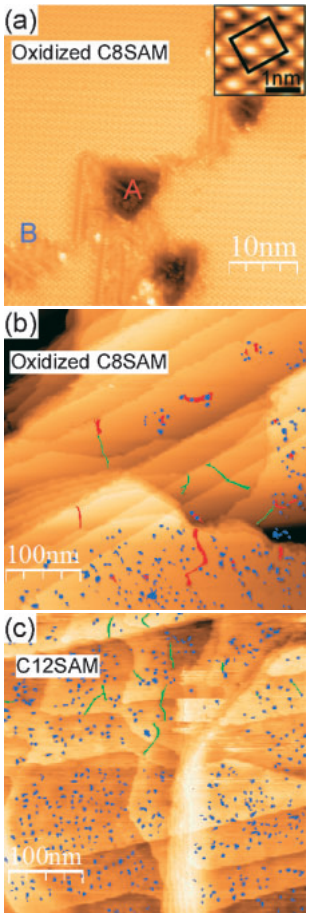

Fig. 1. STM images of (a), (b) oxidized C8SAM/Au and (c) unoxidized C12SAM/Au. Stripe-phase defects, etch pits, and domain boundaries are drawn in red, blue, and green, respectively, in (b) and (c). Inset in (a) shows a magnified area consisting of a $c(4\times2)$ superlattice of a $(\sqrt{3}\times\sqrt{3})R$ 30° lattice.

3.2 STM/STS results of pentacene/alkanethiol/Au

Next, we show results for a pentacene film on a C8-SAM with striped defects. The STS results revealed interesting features different from the topographic results. In Fig. 2(a), stacked pentacene layers with atomically flat terraces can be observed. The step height is 1.6 nm, which corresponds to the interlayer distance of pentacene (001).[15] Figure 2(b) shows I–V and dI/dV curves obtained for different pentacene layers in order of increasing height (from A to F). The dI/dV curves exhibit different gaps, regardless of the energy band gap of pentacene (2.2 eV). Onset voltages (or band-edge voltages) are almost the same in the negative-voltage region, while they are different in the positive-voltage region; the positive onset voltage increases with the layer thickness. These features can be explained by tip-induced band bending (TIBB).[16,17] Owing to the presence of TIBB in the undoped pentacene, the bias voltage applied between the tip and the sample drops in the pentacene layer, and the voltage drop in the tunneling gap becomes lower, resulting in a reduction in tunneling current. Consequently, a higher sample voltage is required for the same amount of current to flow, compared with the case where TIBB does not occur. This causes the onset-voltage shift and apparent gap opening. As the thickness of the pentacene layer is larger, the voltage drop in the layer becomes higher, and the shift in onset voltage increases. Thus, the apparent energy gap is larger than the highest occupied molecular orbital–lowest unoccupied molecular orbital (HOMO–LUMO) gap of pentacene, depending on the layer height of pentacene. Tunneling current starts to flow when the Fermi energy of the tip is equal to the HOMO of pentacene in the positive-sample-voltage region, and to the LUMO of pentacene in the negative-sample-voltage region. Since the Fermi energy of the W tip (work function, 4.8 eV) is much closer to the LUMO than the HOMO of pentacene (affinity, 2.9 eV), the additional voltage required to allow the tunneling current to flow is smaller in the negative-sample-voltage region than

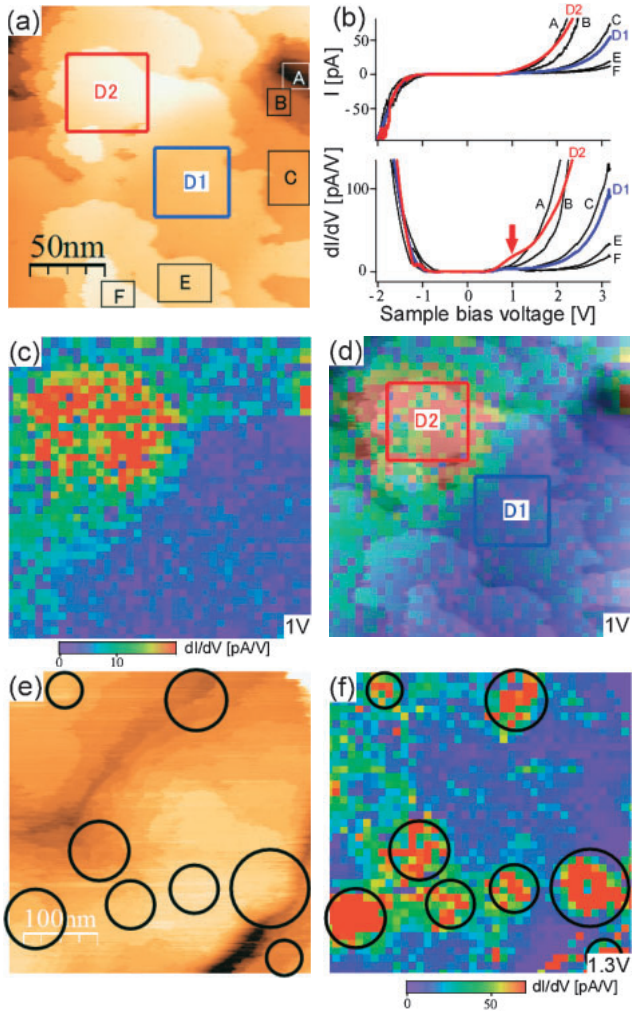

Fig. 2. STS results for pentacene/C8SAM (oxidized)/Au. (a) STM image. (b) *I–V* and dI/dV curves obtained for different areas marked in (a). (c) dI/dV image at 1 V. (d) Overlay of (a) with (c). (e, f) Wide-area STM image and dI/dV image at 1.3 V. The gap-state areas are marked by circles in (e) and (f).

in the positive-sample-voltage region. This leads to the asymmetry of onset voltages observed in Fig. 2(b).

These features are the same as those observed in a previous paper on pentacene on SAMs prepared without oxidation promotion.[18] However, the difference arising from oxidation was clearly observed in the mapping of dI/dV. Figure 2(c) shows a dI/dV image at the sample bias voltage of 1 V. A localized region (with a diameter of about 100 nm) exhibiting much higher values of dI/dV is observed in the upper left of the figure. An image overlaid with the topography [Fig. 2(d)] shows the difference in the dI/dV value from the surface geometry; the dI/dV values measured in the D2 region are different from those measured in the D1 region, although they were measured on the same terrace. As is clear in Fig. 2(b), in the D2 region, the onset voltage shifts toward zero, and a broad peak is observed at 1 V (marked by an arrow in the figure). Since the energy gap shown in the dI/dV curve for the D1 region corresponds to the apparent HOMO–LUMO gap at this layer height, the broad peak is a state in the pentacene band gap (gap state).

To examine the spatial correlation between the gap state and striped defects in SAMs, we compared STM and dI/dV images obtained over a wide area [Figs. 2(e) and 2(f)]. In the figures, the areas where localized gap states are observed in Fig. 2(f) (gap-state areas) are marked by circles. The gap-state area density is estimated to be $1.5 \times 10^{10}\,\mathrm{cm}^{-2}$ from the dI/dV images. This value is close to the stripe-phase density of $2.5 \times 10^{10}\,\mathrm{cm}^{-2}$ and different from the etch-pit density of $4.1 \times 10^{11}\,\mathrm{cm}^{-2}$. This reveals that the gap state is closely related to the stripe defect.

Here, the gap-state areas have no relation with the structures in the topographic image shown in Fig. 2(e). The effect of the defects, which were hidden behind the pentacene overlayers, on the electronic properties of the SAM was clearly observed.

3.3 Discussions on origin of gap state

Let us consider the origin of the gap state. The gap state may originate from defects in pentacene crystalline layers, but this is unlikely for the following reasons. There have been many studies on the electronic structures of defects in organic semiconductors.[3] Vacancies do not form gap states in general. Structural defects accompanied by local lattice strains (such as point defects, dislocations, or grain boundaries) could be the origin of the gap state. However, these are shallow states (located within 0.2 eV from the band edge), and here, we observed no correlation between the topographic features and the gap-state distribution. Thus, these defects could not be the origin of the gap state. Chemical defects arising from a chemical reaction with oxygen or moisture also form gap states. For example, gap states originating from oxygen-related chemical defects are formed at 0.28,[19] 0.38,[20] and 0.6 eV[21] away from the valence band edge of pentacene. These states are located close to the HOMO, which is different from the present case. Thus, the observed gap state is unlikely to originate from defects in pentacene crystalline layers.

On the other hand, in the striped region, alkanethiol molecules are oriented parallel to the surface and do not sufficiently act as a physical isolator, resulting in the formation of a hybrid orbital between pentacene and Au, which could be the origin of the gap state. To confirm this mechanism, we performed STS measurements for a pentacene film on a reference C12-SAM with few striped defects. Figure 3(a) shows an STM image obtained for a pentacene/C12SAM (unoxidized)/Au sample and Fig. 3(b) shows the *I–V* and dI/dV curves obtained for different areas marked in Fig. 3(a). As discussed in §3.2, the shift in positive onset voltage, which depends on the layer height, was observed.

Similarly, a gap state at 2.5 V was observed in region C2, which was not observed in region C1 on the same terrace. In the dI/dV image at 2.5 V [Fig. 3(c)], the gap state is observed only in region C2 and its density is low, in contrast to the case where the SAM with many striped defects was used [Fig. 2(f)]. The other regions exhibiting high dI/dV values are observed (in, for example, region A) because the pentacene layer is thin and the onset voltage is lower than 2.5 V in these regions. For regions with thick layers (around, for example, region D), however, even if the gap state exists, it might not be observed in the dI/dV image at 2.5 V because of the onset voltage shifts due to the large amount of TIBB that occurs on a thick layer. To examine this point, we performed dI/dV measurement at 4 V [Fig. 3(d)]. As is clear

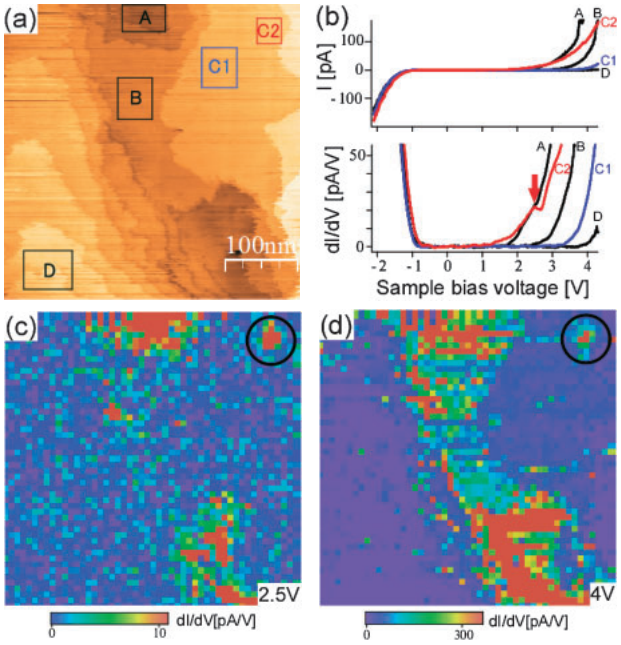

Fig. 3. (a) STS results for pentacene/C12SAM (unoxidized)/Au. (b) *I*–*V* and dI/dV curves obtained for different areas marked in (a). (c, d) dI/dV images for (c) $V_s = 2.5$ and (d) 4 V. The gap-state area is marked by a circle in (c) and (d).

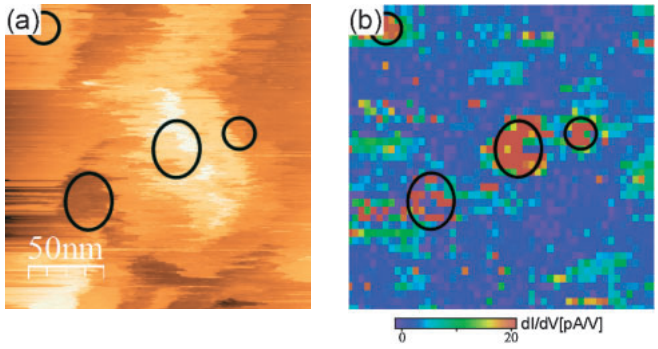

Fig. 4. STS results for petantacene/C12SAM (oxidized)/Au. (a) STM image. (b) dI/dV image at 3.1 V. The gap-state areas are marked by circles.

from the dI/dV image, no localized gap states were observed in D region. In this manner, we investigated the existence of the gap state over the entire surface and confirmed that no gap sates exist except in region C2. From these results, the gap-state density was estimated to be $8.0 \times 10^8\,\mathrm{cm}^{-2}$, which is significantly reduced, as expected. In addition, the reference SAM has many pits and domain boundaries [Fig. 1(c)], and it is confirmed that these pits and boundaries are not related to the formation of the gap state.

Before concluding on the origin of the gap state, we examined the effect of the chain length of the alkanethiol. The crystallinity and resistance to ion penetration increase with SAM thickness.[22] In analogy with this, when a SAM is not sufficiently thick, pentacene molecules may penetrate into it, resulting in the formation of a hybrid orbital. That is, such penetration may occur in the thin C8-SAM but not in the thick C12-SAM, resulting in the difference in gap state density. To exclude this possibility, we examine a pentacene film on a C12-SAM with many striped defects. Figures 4(a) and 4(b) show the STM and dI/dV images at 3.1 V, respectively. Many gap states are observed in Fig. 4(b). The gap-area density is estimated to be $8.3 \times 10^9\,\mathrm{cm}^{-2}$, which is an order of magnitude higher than that in the case where the C12-SAM with few striped defects was used [Figs. 3(c) and 3(d), note the difference in scale]. Thus, it is confirmed that the gap state is mainly due to striped defects, rather than the penetration of pentacene molecules into the SAM crystalline layer.

4. Conclusions

We visualized the spatial correlation between structural defects associated with a gap state in SAM dielectrics and the electronic properties of pentacene/SAM/Au systems on the nanoscale using STM/STS. The gap state was introduced using oxidized alkanthiol molecules based on the formation of a hybrid orbital between pentacene molecules and Au substrate. The gap state hidden behind the pentacene over layers was clearly observed in dI/dV images for a SAM with striped defects, with the distribution unrelated to the topographic features, as expected. These findings suggest that the technique used in this study is applicable to the nanoscale real-space evaluation of the correlation between structural defects in buried dielectrics and the overall performance of organic devices.

1) A. Facchetti, M.-H. Yoon, and T. J. Marks: Adv. Mater. **17** (2005) 1705.
2) D. Vuillaume, C. Boulas, J. Collet, J. V. Davidovits, and F. Rondelez: Appl. Phys. Lett. **69** (1996) 1646.
3) H. Sirringhaus: Adv. Mater. **21** (2009) 3859, and references therein.
4) S. A. DiBenedetto, A. Faccetti, M. A. Ratner, and T. J. Marks: Adv. Mater. **21** (2009) 1407.
5) J. C. Love, L. A. Estroff, J. K. Kriebel, R. G. Nuzzo, and G. M. Whitesides: Chem. Rev. **105** (2005) 1103.
6) R. Schmechel and H. von Seggern: Phys. Status Solidi A **201** (2004) 1215.
7) M. Halik, H. Klauk, U. Zschieschang, G. Schmid, C. Dehm, M. Schütz, S. Maisch, F. Effenberger, M. Brunnbauer, and F. Stellacci: Nature **431** (2004) 963.
8) M. D. Porter, T. B. Bright, D. L. Allara, and C. E. D. Chidsey: J. Am. Chem. Soc. **109** (1987) 3559.
9) C. E. D. Chidsey: Science **251** (1991) 919.
10) G. E. Poirier and E. D. Pylant: Science **272** (1996) 1145.
11) G. E. Poirier: Chem. Rev. **97** (1997) 1117, and references therein.
12) B. V. Palermo, M. Palma, and P. Samori: Adv. Mater. **18** (2006) 145.
13) J. Repp, G. Meyer, S. Paavilainen, F. E. Olsson, and M. Persson: Science **312** (2006) 1196.
14) G. E. Poirirer, T. M. Herne, C. C. Miller, and M. J. Tarlov: J. Am. Chem. Soc. **121** (1999) 9703.
15) C. C. Mattheus, A. B. Dros, J. Baas, G. T. Oostergetel, A. Meetsma, J. L. de Boer, and T. T. M. Palstra: Synth. Met. **138** (2003) 475.
16) L. Kronik and Y. Shapira: Surf. Sci. Rep. **37** (1999) 1.
17) S. Yoshida, Y. Kanitani, R. Oshima, Y. Okada, O. Takeuchi, and H. Shigekawa: Phys. Rev. Lett. **98** (2007) 026802.
18) L. Ruppel, A. Birkner, G. Witte, C. Busse, Th. Lindner, G. Paasch, and Ch. Wöll: J. Appl. Phys. **102** (2007) 033708.
19) W. L. Kalb, K. Mattenberger, and B. Batlogg: Phys. Rev. B **78** (2008) 035334.
20) J. E. Northrup and M. L. Chabinyc: Phys. Rev. B **68** (2003) 041202.
21) V. Nádaždy, R. Durný, J. Puigdollers, C. Voz, S. Cheylan, and K. Gmucová: Appl. Phys. Lett. **90** (2007) 092112.
22) F. P. Zamborini and R. M. Crooks: Langmuir **14** (1998) 3279.